Izvorni znanstveni rad 13
Original scientific paper UDK 624.07:519.6

NATURAL FREQUENCIES OF THE MODERATELY THICK PLATE MODELS WITH UNIFORMLY DISTRUBUTED MASS

VLASTITA TITRANJA MODELA UMJERENO DEBELIH PLOČA S JEDNOLIKO RASPOREĐENOM MASOM

Marin Grbac*, Dragan Ribarić*

Abstract

A four-node finite element is developed for modeling plates according to the Mindlin plate theory and it is constructed with the assumed shear strain approach. The element is previously verified in a static analysis on the benchmark problems of moderately thick and extremely thin plate models and compared to the other elements known from the literature. As starting interpolations, a complete cubic polynomial for the transverse displacement field and quadratic polynomials for the two rotation fields are used, and they are problem dependent at the same time. Some unfavorable terms are excluded from the derived shear strain expression to avoid locking phenomena in the thin geometry conditions. In this paper, the proposed element is tested for the dynamic analysis calculating the natural frequencies of plate vibrations with the uniformly distributed mass. The influence of the element consistent mass matrix is analyzed on the first 12 vibration modes. The results are verified on the circular plate model and compared to the existing analytical solutions as well as the results of other four-node elements from the literature. The goal of this paper is to demonstrate the efficiency of the proposed assumed strain element also in the dynamic analysis of plane structures.

Key words: *Mindlin plate theory, finite elements, assumed natural strains, problem dependent linked interpolations, plate natural frequencies, consistent mass matrix*

Sažetak

Četveročvorni konačni element za numeričko modeliranje ploča po Mindlinovoj teoriji razvijen je s usvojenim interpolacijama polja smicanja te je, u usporedbi s drugim

* University of Rijeka, Faculty of Civil Engineering, Radmile Matejčić 3, 51000 Rijeka
E-mail: {marin.grbac,dragan.ribaric}@uniri.hr

10. 11. 2018. 7. 1. 2019.

poznatim konačnim elementima iz literature, pokazao vrlo dobro ponašanje pri statičkoj analizi umjereno debelih, ali i vrlo tankih ploča. Polazne interpolacijske funkcije ovog pločastog elementa su potpuni kubni polinom za polje transverzalnih pomaka i kvadratni za polja rotacija presjeka, ali su pri tome same interpolacije na kubnoj razini ovisne o materijalnim vrijednostima („problem dependent"). Derivirani izraz za deformacije smicanja je potom reduciran za one članove koji uzrokuju pojavu „lockinga" (loše konvergencije) kod modela vrlo tankih ploča. U ovom radu takav model elementa proširen je za primjenu na dinamičku analizu pločastih modela, odnosno određivanja vlastitih frekvencija titranja ploča okomito na ravninu modela uz jednoliko distribuiranu masu ploče. Analiziran je utjecaj konzistentno zadane matrice masa na vrijednosti prvih 12 tonova prirodnih frekvencija. Rezultati su verificirani na modelu kružne ploče za koji postoje analitička rješenja te su uspoređeni i s rezultatima drugih efikasnih četveročvornih elemenata iz literature. Ovim radom želi se pokazati da je analizirani četveročvorni konačni element efikasan i konkurentan i za primjenu na dinamičke probleme koji se mogu pojaviti u projektiranju površinskih konstrukcija.

Ključne riječi: *Mindlinova teorija ploča, konačni elementi, usvojene prirodne deformacije, vezane interpolacije ovisne o problemu, vlastite frekvencije ploča, konzistentna matrica masa*

1. Introduction

The finite element method is a powerful tool for solving a variety of mechanical problems involving solids, shells, plates, membranes and bars of various types. The mechanical model is discretized by a set of finite elements and the approximate solution is calculated as the result of linearized equations. The question if the solution is close enough to the exact result is inevitable. Of course, if the model is composed of an appropriate number of elements with dense node meshes, the solution will be in the margin of tolerable errors, but great efforts have been made by researchers to develop finite elements able to approximate exact solutions on coarse meshes with as few elements possible.

Here, we propose a novel finite element for modeling of moderately thick plates that is designed on the so-called assumed strain concept. This concept was introduced by Hughes and Tezduyar in [1] and applied on the quadrilateral element for the "Kirchhoff mode" of quadratic order. The idea was exploited afterwards by MacNeal [2] and by Bathe and Dvorkin [3] on the Mindlin type quadrilaterals. They assumed that linear shear strain fields correct deficiencies of the isoparametric method and avoid spurious shear strains on irregular element shapes. MacNeal concluded that for n-node element the number of the independent transverse shear coefficients to prevent spurious mechanisms is equal to n. Bathe and Dvorkin used the same assumption for the shear but they interpreted it as the covariant

tensor components. Their four-node elements are known in literature as *QUAD4* and *MITC4* respectively.

Since then, many improvements have been attempted and the presented four-node element is one of the kind. This element starts with the full cubic polynomial interpolation for the plate transverse displacement and quadratic for the two global plate section rotations and captures only favorable terms in the shear strain expressions meaning that the shears are assumed to control convergences. The element is already tested on the variety of benchmark examples, and compared to the other efficient elements from the literature. In this paper, the abilities of the element are demonstrated on the dynamical benchmark problem of solving first few vibration modes for the clamped circular plate with uniform thickness, where an irregular mesh is inevitable and for which the analytical exact solution exists and can be used for comparison.

2. New four-node Mindlin-type plate element

Firstly, we want to describe a new four-node quadrilateral element designed to model plate problems according to the Mindlin plate theory, meaning that the bending, as well as the shear strains are involved in the stiffness matrix assemblage. The element describes the plate with uniform thickness t, with material parameters: E, the elasticity modulus, G, the shear modulus, ν, the Poisson's ratio and k, the section shear correction factor usually taken as $k=5/6$ for plates.

2.1. Interpolations for a four-node element

First, we choose an interpolation of the transverse displacement field (w). A quadratic polynomial [4] or a cubic polynomial [5] are good options for the later derivation of the assumed shear strain field. At the same time, the interpolations for the two section-rotation fields (θ_x and θ_y) have to be polynomials of one order lower than those used for interpolation of transverse displacements. See [4] and [5] for details, where the evolution of this assumption has been explained.

If a quadratic polynomial is used to interpolate displacement over the element domain, nine terms of the Pascal's triangle must be engaged and associated with some degrees of freedom to satisfy polynomial completeness. All existing nodal parameters $w_1,\ldots,w_4$, $\theta_{x1},\ldots,\theta_{x4}$, $\theta_{y1},\ldots,\theta_{y4}$, are involved together with one extra internal parameter w_{Bb0} (regarded as an internal bubble displacement parameter).

If a cubic polynomial is chosen, another seven cubic function items have to be added in the displacement interpolation and seven more parameters should be associated. Four of them are the element-side curvature

increments $\Delta\kappa_{ij}$ according to the differential equation solution of the two-node beam element and the last three are cubic internal parameters w_{Bb3}, w_{Bb4} and w_{Bb5} that do not affect the conformity of the displacement field at the connection with adjacent elements.

At the same time, the associated section-rotation fields should also be expanded to the quadratic order adding five new items to each of them. The associated parameters include four projections of the curvature increments and the fifth is a rotation bubble parameter different for each field, namely θ_{Bb1} and θ_{Bb2}.

The final cubic interpolation for the transverse displacement reads:

$$
\begin{aligned}
w = {} & \frac{1-\xi}{2}\frac{1-\eta}{2}w_1 + \frac{1+\xi}{2}\frac{1-\eta}{2}w_2 + \frac{1+\xi}{2}\frac{1+\eta}{2}w_3 + \frac{1-\xi}{2}\frac{1+\eta}{2}w_4 \\
& + \frac{1-\xi^2}{4}\frac{1-\eta}{2}\frac{1}{2}\left[(\theta_{y2}-\theta_{y1})(x_2-x_1)-(\theta_{x2}-\theta_{x1})(y_2-y_1)\right] \\
& + \frac{1-\xi^2}{4}\frac{1+\eta}{2}\frac{1}{2}\left[(\theta_{y3}-\theta_{y4})(x_3-x_4)-(\theta_{x3}-\theta_{x4})(y_3-y_4)\right] \\
& + \frac{1+\xi}{2}\frac{1-\eta^2}{4}\frac{1}{2}\left[(\theta_{y3}-\theta_{y2})(x_3-x_2)-(\theta_{x3}-\theta_{x2})(y_3-y_2)\right] \\
& + \frac{1-\xi}{2}\frac{1-\eta^2}{4}\frac{1}{2}\left[(\theta_{y4}-\theta_{y1})(x_4-x_1)-(\theta_{x4}-\theta_{x1})(y_4-y_1)\right] \\
& + \frac{1-\xi^2}{4}\frac{1-\eta^2}{4}w_{Bb0} \\
& - \frac{\xi-\xi^3}{4}\frac{1-\eta}{2}\Delta\kappa_{12}\frac{L_{12}^2}{6} - \frac{1+\xi}{2}\frac{\eta-\eta^3}{4}\Delta\kappa_{23}\frac{L_{23}^2}{6} \\
& + \frac{\xi-\xi^3}{4}\frac{1+\eta}{2}\Delta\kappa_{34}\frac{L_{34}^2}{6} + \frac{1-\xi}{2}\frac{\eta-\eta^3}{4}\Delta\kappa_{41}\frac{L_{41}^2}{6} \\
& + \frac{\xi-\xi^3}{4}\frac{1-\eta^2}{4}\frac{1}{3}w_{Bb,3} + \frac{1-\xi^2}{4}\frac{\eta-\eta^3}{4}\frac{1}{3}w_{Bb,4} + \frac{\xi-\xi^3}{4}\frac{\eta-\eta^3}{4}\frac{1}{3}w_{Bb,5}, \qquad (1)
\end{aligned}
$$

The first line in (1) is a bilinear Lagrangian interpolation among nodal displacement parameters $w_1,\ldots,w_4$ and the five following lines complete the quadratic linked interpolation form [4], involving global nodal rotations $\theta_{x1},\ldots,\theta_{x4}$, and $\theta_{y1},\ldots,\theta_{y4}$, together with the extra internal quadratic bubble displacement parameter w_{Bb0}. The seventh and the eighth line are cubic

interpolation expansions related to the side curvature increments $\Delta\kappa_{ij}$ that can be expressed as problem dependent parameters associated with the existing nodal displacements and rotations. For example, for the element side connecting node 1 to node 2, the side curvature increment $\Delta\kappa_{12}$ is proportional to the expression for shear strain (in brackets):

$$\Delta\kappa_{12} = -\left(w_2 - w_1 - \frac{\theta_{x1}+\theta_{x2}}{2}\cdot(y_2 - y_1) + \frac{\theta_{y1}+\theta_{y2}}{2}\cdot(x_2 - x_1) \right) \frac{1}{1+\dfrac{12D}{L_{12}^2(Gtk)}} \frac{6}{L_{12}^2} \tag{2}$$

In the expressions (1) and (2) L_{12} denotes the element side length (in general L_{ij} denotes any other element side length connecting node *i* to node *j*). D is the plate bending rigidity, $D=Et^3/(12(1-\nu^2))$ and Gtk is the shear rigidity. The final line in (1) completes the cubic expansion with the new inner-element bubble parameters w_{Bb3}, w_{Bb4} and w_{Bb5}.

Rotation fields, which are linked to the transverse displacement interpolation (1), are interpolated separately with quadratic polynomials:

$$\begin{aligned}\theta_x = \sum_{i=1}^{4} N_i\theta_{xi} &- \frac{1-\xi^2}{4}\frac{1-\eta}{2}\Delta\kappa_{12}(y_2 - y_1) - \frac{1+\xi}{2}\frac{1-\eta^2}{4}\Delta\kappa_{23}(y_3 - y_2) \\ &- \frac{1-\xi^2}{4}\frac{1+\eta}{2}\Delta\kappa_{34}(y_4 - y_3) - \frac{1-\xi}{2}\frac{1-\eta^2}{4}\Delta\kappa_{41}(y_1 - y_4) \\ &- \frac{1-\xi^2}{4}\frac{1-\eta^2}{4}\theta_{Bb,1}\end{aligned} \tag{3}$$

$$\begin{aligned}\theta_y = \sum_{i=1}^{4} N_i\theta_{yi} &+ \frac{1-\xi^2}{4}\frac{1-\eta}{2}\Delta\kappa_{12}(x_2 - x_1) + \frac{1+\xi}{2}\frac{1-\eta^2}{4}\Delta\kappa_{23}(x_3 - x_2) \\ &+ \frac{1-\xi^2}{4}\frac{1+\eta}{2}\Delta\kappa_{34}(x_4 - x_3) + \frac{1-\xi}{2}\frac{1-\eta^2}{4}\Delta\kappa_{41}(x_1 - x_4) \\ &+ \frac{1-\xi^2}{4}\frac{1-\eta^2}{4}\theta_{Bb,2}\end{aligned} \tag{4}$$

Here the Lagrangian interpolation functions denoted by N_i are identical as in the first line of (1), but associated with the global nodal rotations. $\Delta\kappa_{ij}$ are identical side curvature increments as in (2), but multiplied with the element side projections, while θ_{Bb1} and θ_{Bb2} are again the internal bubble parameters of the rotation fields that complete the quadratic polynomial form.

In total, all three fields are interpolated with 12 nodal parameters (degrees of freedom) and with 6 internal parameters that can be statically condensed at the end of the stiffness matrix formation process.

2.2. Assumed shear strain field

The shear strains in global directions γ_x and γ_y for the Mindlin plate assumptions follow the kinematics:

$$\gamma_x = \frac{dw}{dx} + \theta_y \text{ and } \gamma_y = \frac{dw}{dy} - \theta_x, \tag{5}$$

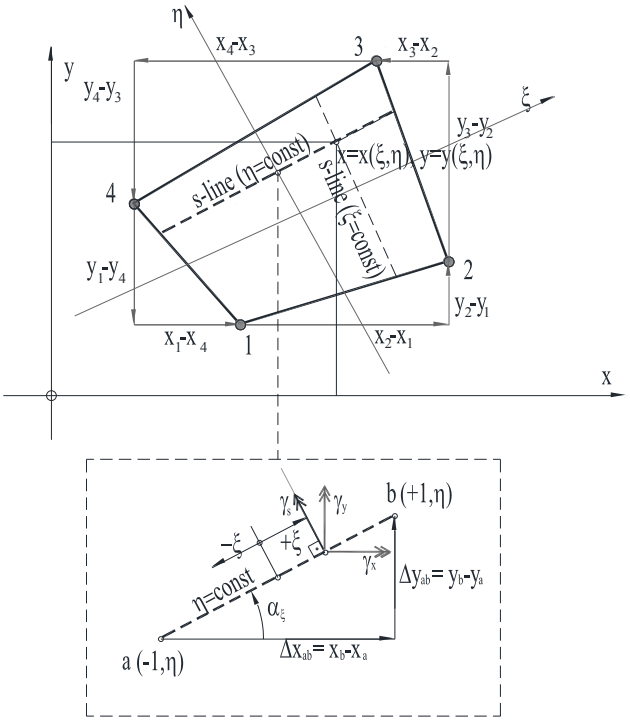

Figure 1. Arbitrary 4-node quadrilateral plate element – relations between shear strains in the global and in the natural coordinates

as well as constitutive relations:

$$\gamma_x = \frac{V_x}{Gtk} \text{ and } \gamma_y = \frac{V_y}{Gtk}, \tag{6}$$

where V_x and V_y are the shear stress resultants.

If alternatively, shear strains are formulated for the element natural coordinates, then the line "s" passing through an arbitrary inner point with constant η, is taken into the consideration (Fig. 1). The shear strain $\gamma_{s,\xi}$ can now be expressed with respect to the global shear strains as

$$\gamma_{s,\xi} = \gamma_x \cos\alpha_\xi + \gamma_y \sin\alpha_\xi = \left(\frac{\partial w}{\partial x} + \theta_y\right)\cos\alpha_\xi + \left(\frac{\partial w}{\partial y} - \theta_x\right)\sin\alpha_\xi$$

$$= \frac{\partial w}{\partial x}\cos\alpha_\xi + \frac{\partial w}{\partial y}\sin\alpha_\xi + \theta_y\cos\alpha_\xi - \theta_x\sin\alpha_\xi = \frac{\partial w}{\partial s} + \theta_{ns}, \tag{7}$$

meaning that it can be computed as a sum of the derivative of displacement field (1) with respect to s, and the rotational fields (2) and (3) projected to the normal on the "s" line [6].

$$\gamma_{s,\xi} = \left\{\frac{1-\eta}{2}\left(\frac{w_2 - w_1}{2} + \frac{\theta_{y1}+\theta_{y2}}{2}\cdot\frac{x_2 - x_1}{2} - \frac{\theta_{x1}+\theta_{x2}}{2}\cdot\frac{y_2 - y_1}{2} + \Delta\kappa_{12}\frac{L_1^2}{12}\right) -\right.$$

$$-\frac{1+\eta}{2}\left(\frac{w_4 - w_3}{2} + \frac{\theta_{y3}+\theta_{y4}}{2}\cdot\frac{x_4 - x_3}{2} - \frac{\theta_{x3}+\theta_{x4}}{2}\cdot\frac{y_4 - y_3}{2}\right.$$

$$\left.\left. + \Delta\kappa_{34}\frac{L_3^2}{12}\right) +\right.$$

$$+\frac{1-\eta^2}{4}\left[\frac{\theta_{y3}-\theta_{y2}}{2}\cdot\frac{x_4 - x_1}{2} - \frac{\theta_{y4}-\theta_{y1}}{2}\cdot\frac{x_3 - x_2}{2} - \frac{\theta_{x3}-\theta_{x2}}{2}\cdot\frac{y_4 - y_1}{2} + \frac{\theta_{x4}-\theta_{x1}}{2}\cdot\frac{y_3 - y_2}{2} +\right.$$

$$+\frac{\Delta\kappa_{23}}{2}\left((y_3 - y_2)\frac{(y_2 - y_1)-(y_4 - y_3)}{4} + (x_3 - x_2)\frac{(x_2 - x_1)-(x_4 - x_3)}{4}\right) +$$

$$\left.+\frac{\Delta\kappa_{41}}{2}\left((y_1 - y_4)\frac{(y_2 - y_1)-(y_4 - y_3)}{4} + (x_1 - x_4)\frac{(x_2 - x_1)-(x_4 - x_3)}{4}\right) - \frac{w_{Bb,3}}{6}\right] +$$

$$+\frac{\xi}{2}\frac{1-\eta^2}{4}\left[(\theta_{x1} - \theta_{x2} + \theta_{x3} - \theta_{x4})\frac{\Delta y}{2} - (\theta_{y1} - \theta_{y2} + \theta_{y3} - \theta_{y4})\frac{\Delta x}{2} - w_{Bb,0} +\right.$$

$$+\Delta\kappa_{23}\left((y_3 - y_2)\frac{(y_2 - y_1)-(y_4 - y_3)}{4} + (x_3 - x_2)\frac{(x_2 - x_1)-(x_4 - x_3)}{4}\right) -$$

$$\left.-\Delta\kappa_{41}\left((y_1 - y_4)\frac{(y_2 - y_1)-(y_4 - y_3)}{4} + (x_1 - x_4)\frac{(x_2 - x_1)-(x_4 - x_3)}{4}\right)\right] +$$

$$+\frac{1-\xi^2}{4}\frac{1-\eta^2}{4}\left[\Delta\kappa_{12}\left((y_2 - y_1)\frac{\Delta y}{2} + (x_2 - x_1)\frac{\Delta x}{2}\right) -\right.$$

$$-\Delta\kappa_{34}\left((y_4-y_3)\frac{\Delta y}{2}+(x_4-x_3)\frac{\Delta x}{2}\right)+$$

$$+\theta_{Bb,1}\frac{(y_2-y_1)-(y_4-y_3)}{4}+\theta_{Bb,2}\frac{(x_2-x_1)-(x_4-x_3)}{4}+w_{Bb,3}\Bigg]+$$

$$+\frac{1}{2}\frac{\eta-\eta^3}{4}\Bigg[\Delta\kappa_{23}\left(\frac{L_2^2}{12}+\frac{(x_3-x_2)(x_1-x_4)}{4}+\frac{(y_3-y_2)(y_1-y_4)}{4}\right)+$$

$$+\Delta\kappa_{41}\left(\frac{L_4^2}{12}+\frac{(x_3-x_2)(x_1-x_4)}{4}+\frac{(y_3-y_2)(y_1-y_4)}{4}\right)-w_{Bb,5}\frac{1}{3}\Bigg]+$$

$$+\frac{\xi}{2}\frac{\eta-\eta^3}{4}\Bigg[\Delta\kappa_{23}\left((y_3-y_2)\frac{\Delta y}{2}+(x_3-x_2)\frac{\Delta x}{2}\right)-$$

$$-\Delta\kappa_{41}\left((y_1-y_4)\frac{\Delta y}{2}+(x_1-x_4)\frac{\Delta x}{2}\right)-w_{Bb,4}\frac{1}{3}\Bigg]+$$

$$+\frac{1-\xi^2}{4}\frac{\eta-\eta^3}{4}\left(\theta_{Bb,1}\frac{\Delta y}{4}+\theta_{Bb,2}\frac{\Delta x}{4}+w_{Bb,5}\right)\Bigg\}\frac{1}{\frac{\partial s}{\partial\xi}}. \qquad (8)$$

Similar expression for $\gamma_{s,\eta}$ can be formulated for "s" line passing through an arbitrary inner point with constant variable ξ (see [6]).

2.3. The patch test

The ability of the elements to produce exact stresses and to accommodate exact displacement is usually tested on the patchwork of irregular elements framed in a rectangular domain. A simple stress condition of constant cylindrical bending is assumed. On the outer nodes, all displacement and rotation degrees of freedom are prescribed and exact solution for the inner nodes is expected together with the exact stresses in the integration points of all elements.

It has been already demonstrated [7] that quadratic linked interpolation part from (1), (3) and (4) is sufficient to pass the cylindrical bending test on the patchwork geometry with constant field for moments and zero shear forces. Full cubic interpolation from (1), (3) and (4) also passes the patch test since all higher order terms are zeroed by the minimization procedure on the total energy of the problem [5].

Nevertheless, a pure displacement based element constructed with only the described interpolations exhibits locking phenomena with coarse meshes and for very thin geometries.

Note that shear strain expression (8) is in neat contrast with the bending strain expressions [6] regarding equilibrium relations on one side and the actual polynomial order on the other. Therefore, in (8) any term associated with functions of the higher order then linear (any after the first two lines in (8)) can be omitted in the assumed shear expression as well as any cubic expansion parameter (including bubbles), with no effect on the ability to pass the constant bending patch test where shear should be zero.

After careful analysis, the best results are achieved by eliminating (or subtracting) only the parameter in the third line of (8). The shear strain part $\Delta\gamma_{s,\xi}$ that makes the displacement based element too stiff is

$$\Delta\gamma_{s,\xi} = \frac{1-\eta^2}{4}\left[\frac{\theta_{y3}-\theta_{y2}}{2}\cdot\frac{x_4-x_1}{2} - \frac{\theta_{y4}-\theta_{y1}}{2}\cdot\frac{x_3-x_2}{2} - \right.$$
$$\left. - \frac{\theta_{x3}-\theta_{x2}}{2}\cdot\frac{y_4-y_1}{2} + \frac{\theta_{x4}-\theta_{x1}}{2}\cdot\frac{y_3-y_2}{2}\right], \tag{9}$$

and will be excluded from the final expression for the shear strain $\gamma_{s,\xi}$.

Similarly, for expression $\gamma_{s,\eta}$ with constant natural coordinate ξ, we get the best results in avoiding locking phenomena by subtracting the following shear strain part:

$$\Delta\gamma_{s,\eta} = -\frac{1-\xi^2}{4}\left[\frac{\theta_{y3}-\theta_{y4}}{2}\cdot\frac{x_2-x_1}{2} - \frac{\theta_{y2}-\theta_{y1}}{2}\cdot\frac{x_3-x_4}{2}\right.$$
$$\left. - \frac{\theta_{x3}-\theta_{x4}}{2}\cdot\frac{y_2-y_1}{2} + \frac{\theta_{x2}-\theta_{x1}}{2}\cdot\frac{y_3-y_4}{2}\right]. \tag{10}$$

The result of this reduction is the assumed form for the shear strains for a new element that will become of the mixed type, but with the stiffness matrix assembled by involving only the strain functionals.

More details about the assumed strain four-node element can be found in [6].

3. Stiffness and mass matrix

To determine the natural frequencies of the structural system, the homogeneous equation of the form

$$\mathbf{K}_s\mathbf{p}_s + \mathbf{M}_s\ddot{\mathbf{p}}_s = \mathbf{0} \tag{11}$$

has to be solved, with $\mathbf{K}_s$ as the global stiffness matrix and $\mathbf{M}_\mathbf{s}$ as the global mass matrix, while $\mathbf{p}_s$ is the vector of global nodal degrees of freedom with $\ddot{\mathbf{p}}_s$ its second derivative in time.

The global stiffness matrix $\mathbf{K}_s$ is assembled from stiffness matrices $\mathbf{K}_e$ of all elements in the standard minimization process of the total potential energy. The element stiffness matrix is formed with two independent contributions, the bending energy part and the shear energy part (Mindlin theory assumption):

$$\mathbf{K}_\mathbf{e} = \mathbf{K}_B + \mathbf{K}_S = \int_{Ae} \mathbf{B}_B^T \cdot \mathbf{D}_B \cdot \mathbf{B}_B dA + \int_{Ae} \mathbf{B}_S^T \cdot \mathbf{D}_S \cdot \mathbf{B}_S dA\,, \tag{12}$$

where the curvature strains and the shear strains are expressed with so-called $\mathbf{B}$ matrices via element nodal degrees of freedom $\mathbf{p}_e$:

$$\boldsymbol{\kappa} = \mathbf{B}_B \mathbf{p}_e\,, \tag{13}$$

$$\boldsymbol{\gamma} = \mathbf{B}_S \mathbf{p}_e\,, \tag{14}$$

and where $\mathbf{D}_B$ and $\mathbf{D}_S$ are the constitutive matrices for bending and shear respectively

$$\mathbf{D}_B = \frac{Et^3}{12(1-\nu^2)} \begin{bmatrix} 1 & \nu & 0 \\ \nu & 1 & 0 \\ 0 & 0 & \dfrac{1-\nu}{2} \end{bmatrix} \quad \mathbf{D}_S = Gtk \begin{bmatrix} 1 & 0 \\ 0 & 1 \end{bmatrix}. \tag{15}$$

The mass matrix is calculated from the element mass matrices $\mathbf{M}_{C,e}$ as fully populated consistent mass matrices integrated using the standard finite element procedure [8]:

$$\mathbf{M}_{C,\mathbf{e}} = \int_{Ae} \mathbf{N}_w^T \mathbf{N}_w \rho \cdot t dA + \int_{Ae} \mathbf{N}_{\theta x}^T \mathbf{N}_{\theta x} \rho \cdot \frac{t^3}{12} dA + \int_{Ae} \mathbf{N}_{\theta y}^T \mathbf{N}_{\theta y} \rho \cdot \frac{t^3}{12} dA\,. \tag{16}$$

ρ in (16) is a volume unit mass, t is the plate-section thickness, while $\mathbf{N}_w$ is a vector of all shape functions associated with the nodal displacement w in (1), $\mathbf{N}_{\theta x}$ a vector of all shape functions associated with the nodal rotation θ_x in (3) and $\mathbf{N}_{\theta y}$ a vector of all shape functions associated with the

nodal rotation θ_y in (4), since (1), (3) and (4) can be rewritten in matrix forms

$$w = \mathbf{N}_w \mathbf{p}_e , \tag{17}$$

$$\theta_x = \mathbf{N}_{\theta x} \mathbf{p}_e , \tag{18}$$

$$\theta_y = \mathbf{N}_{\theta y} \mathbf{p}_e . \tag{19}$$

$\mathbf{p}_e$ in (17), (18) and (19) is again a vector of all element nodal degrees of freedom.

If the homogenous global model solution for $\mathbf{p}_{s,\omega}$ in time is assumed, equation (11) can be simplified to the generalized eigenvalue equation

$$\left(\mathbf{K}_s - \omega^2 \mathbf{M}_s\right) \cdot \mathbf{p}_{s,\omega} = \mathbf{0}, \tag{20}$$

where ω is an eigenvalue representing the circular natural frequency of the problem vibration and $\mathbf{p}_{s,\omega}$ is the eigenvector of that vibration. Number of the problem eigenvalues ω_i are equal to the number of non-zero global nodal degrees of freedom, but usually only the lowest few are checked and are the most accurate.

4. A numerical example

A circular plate with the perimeter clamped support conditions of uniform thickness *t* and uniform mass (Fig. 2) is analyzed and the eigenvalues and eigen shape modes are determined. The geometrical properties used are given in consistent units: radius of the circle, *R=5.0 m* (*2R=10.0 m*) and two thickness conditions, *t=1.0 m* or *t=0.1 m* representing moderately thick and thin model slenderness, respectively. The material properties used are: the elasticity modulus, $E=2.0*10^{11}$ *Pa*, the Poisson's coefficient, *ν=0.3* and the plate volume mass, $\rho=8000.0$ *kg/m*^{3}.

Finite element mesh for the circular plate is symmetric with respect to both principal axes and in every quarter there are either 3 (very coarse mesh), 12 (moderately coarse mesh as shown in Fig. 2) or 48 elements (moderately dense mesh). First 12 eigenvalues of the model with a thick (*t/2R= 0.1*) and a thin (*t/2R= 0.01*) slenderness are calculated according to the procedure embedded in the finite element software FEAP. Their results are given in the Tables 1 to 3 and Figs. 3 to 6. First 8 mode shapes for the circular plate are depicted in Fig. 5. Some eigenvalues are coming in identical pairs but they belong to different anti-symmetric eigen-vectors.

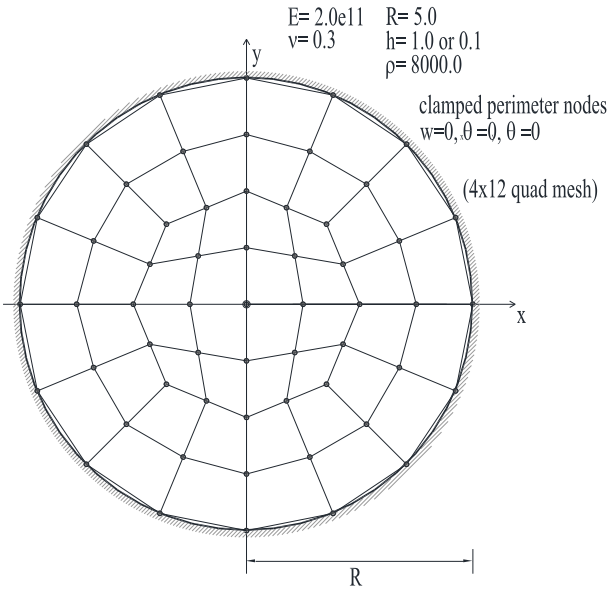

Figure 2. Clamped circular plate and the mesh with 12 elements in a quarter of the circle

Table 1 compares the eigenvalues of all three mesh densities calculated with the present element denoted as *Q4U3-AS* (four node element with cubic interpolations and assumed natural strain). Percentage of errors for the eigenvalues with respect to the analytical solutions are presented in Fig. 3.

Tables 2 and 3 compare the eigenvalues of the present element with the elements from the literature. *MIN3* is a Tessler's and Hughes's three-node Mindlin plate element with improved transverse shear [9], *ANS4* is a Lee's four node element also constructed with the assumed natural shear strain concept [10] and *CS-DSG3* is a triangular element form [11] modelled with the cell-based smoothed discrete shear gap method.

The results from [11] in Tables 2 and 3 are obtained for the plate discretized by the mesh of 394 triangular elements and 222 nodes, while for the present element *Q4U3-AS* the results are obtained with the comparable mesh of 192 quadrilateral elements and 209 nodes.

The error of the results for all elements from Table 2 are presented in Fig. 4 while from Table 3 are presented in Fig. 5.

Table 1. *Clamped circular plate. Convergence of results for various mesh densities of the 12 lowest parameterized natural frequencies,* $\varpi = \omega R^2 \sqrt{\rho \cdot t / D}$ *with slenderness ratio t/2R=0.1*

Mode	Q4U2-AS (4x3 mesh)	Q4U2-AS (4x12 mesh)	Q4U2-AS (4x48 mesh)	Exact [11]
1	9.525	9.320	9.320	9.240
2	19.154	18.055	18.051	17.834
3	19.154	18.055	18.051	17.834
4	30.288	27.302	27.511	27.214
5	30.460	27.436	27.551	27.214
6	40.130	32.176	31.236	30.211
7	46.317	37.330	37.601	37.109
8	46.317	37.330	37.602	37.109
9	63.337	46.128	44.171	42.409
10	63.341	46.128	44.172	42.409
11	67.204	48.204	48.158	47.340
12	81.791	48.438	48.284	47.340

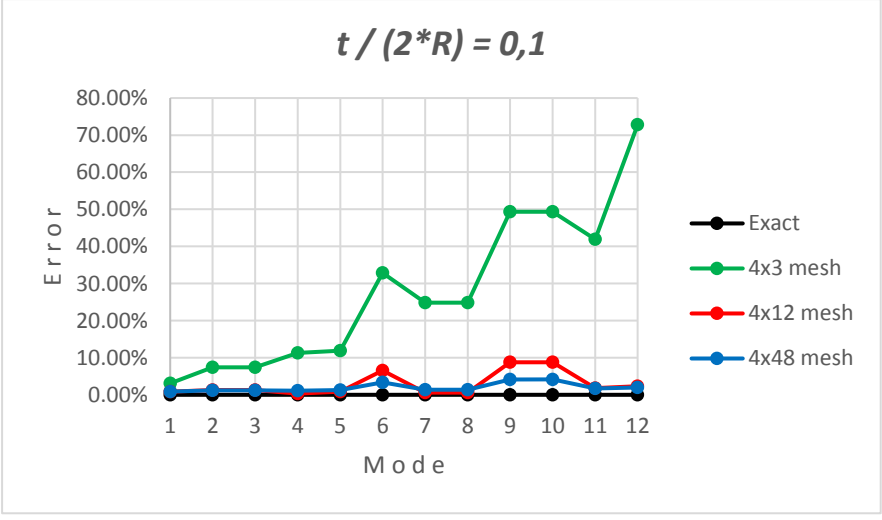

Figure 3. Clamped circular plate. Percentage of the error for the first 12 eigenvalues for the three mesh densities.

Table 2. *Clamped circular plate. 12 lowest parameterized natural frequencies,* $\varpi = \omega R^2 \sqrt{\rho \cdot t / D}$ *for the slenderness ratio t/2R=0.1. Comparison with the exact solution and the results from the literature.*

Mode	MIN3	ANS4	CS-DGS3	Q4U2-AS (Present)	Exact [11]
1	9.968	9.261	9.277	9.320	9.240
2	20.306	17.947	17.802	18.051	17.834
3	20.326	17.947	17.810	18.051	17.834
4	32.780	27.035	27.065	27.511	27.214
5	32.791	27.657	27.080	27.551	27.214
6	37.159	30.322	30.437	31.236	30.211
7	47.544	37.258	36.773	37.601	37.109
8	47.599	37.258	36.853	37.602	37.109
9	55.353	43.270	42.410	44.171	42.409
10	55.661	43.270	42.543	44.172	42.409
11	64.934	47.707	46.667	48.158	47.340
12	64.995	47.803	46.786	48.284	47.340

Table 3. *Clamped circular plate. 12 lowest parameterized natural frequencies,* $\varpi = \omega R^2 \sqrt{\rho \cdot t / D}$ *for the slenderness ratio t/2R=0.01. Comparison with the exact solution and the results from the literature.*

Mode	MIN3 [11]	ANS4	CS-DGS3	Q4U2-AS (Present)	Exact [11]
1	10.4082	10.2572	10.2478	10.1837	10.2158
2	22.2198	21.4981	21.3092	21.1222	21.2600
3	22.2444	21.4981	21.3246	21.1224	21.2600
4	37.7461	35.3941	35.0852	34.2582	34.8800
5	37.7816	35.5173	35.1137	34.3567	34.8800
6	43.0344	40.8975	40.3370	39.6105	39.7710
7	57.8881	52.2054	51.6052	49.5884	51.0400
8	58.0836	52.2054	51.7926	49.5892	51.0400
9	68.7260	63.2397	61.7079	60.2619	60.8200
10	69.2354	63.2397	62.0897	60.2634	60.8200
11	84.3603	71.7426	71.0569	66.7670	69.6659
12	84.4507	72.0375	71.3304	67.0462	69.6659

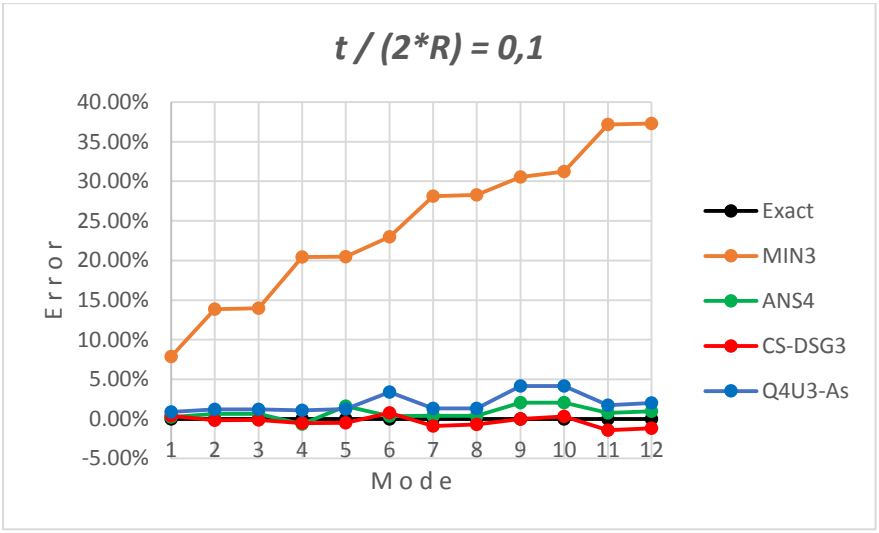

Figure 4. Clamped circular plate. Percentage of the error in the first 12 eigenvalues of the presented element compared with the errors of the elements from literature. Referred to the slenderness t/2R=0.1.

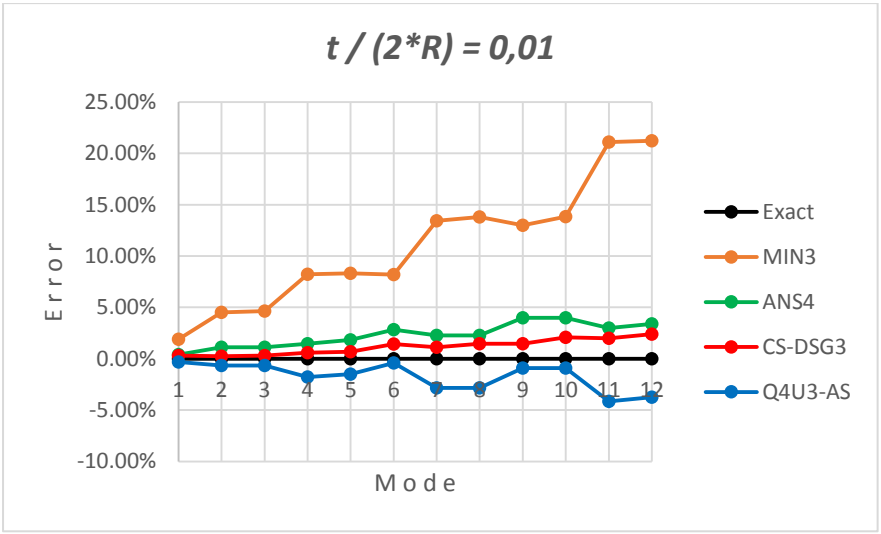

Figure 5. Clamped circular plate. Percentage of the error in the first 12 eigenvalues of the presented element compared with the errors of the elements from literature. Referred to the slenderness t/2R=0.01.

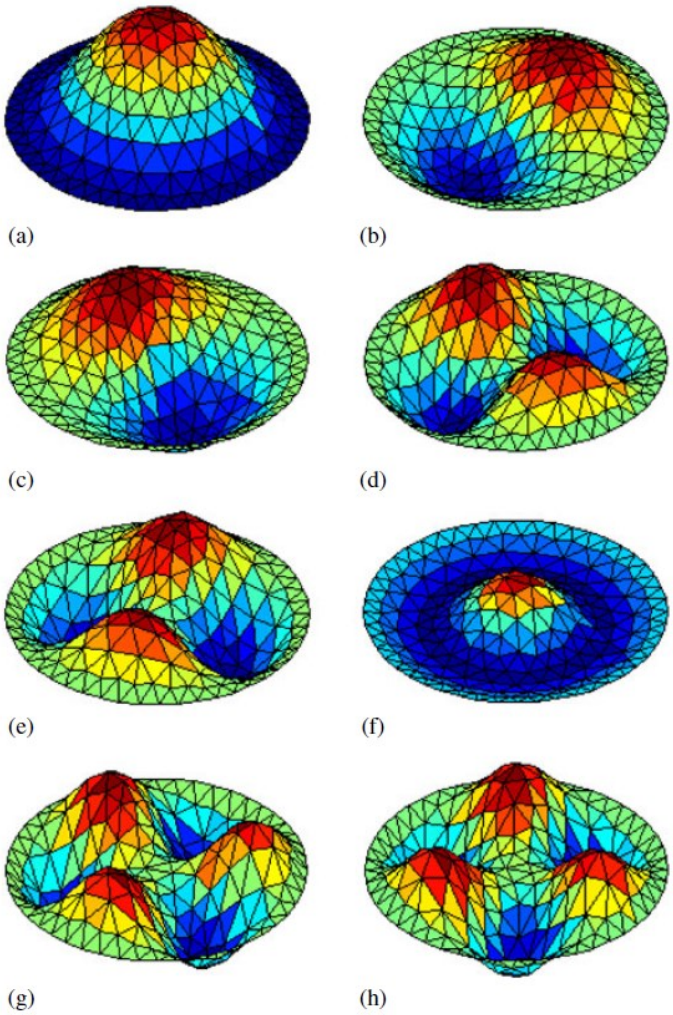

Figure 6. Clamped circular plate. Shape of eight lowest eigen modes [11]. (a) mode 1, (b)-(c) modes 2 and 3, (d)-(e) modes 4 and 5, (f) mode 6, (g)-(h) modes 7 and 8.

In Table 1 (Fig. 3), a frequency deviation in 6^{th}, 9^{th} and 10^{th} mode can be observed. Similar behavior but in smaller scale can be observed for other elements from the literature (Figs. 4 and 5). We attribute this deviation to the pattern of the model meshes, which all have to pass from the radial shape on the model perimeter to the quasi rectangle shape around the plate center. The concerned modal shapes are more influenced than the other ones.

Nevertheless, the results obtained for the present element are quite satisfactory and comparable to other relevant elements from the literature.

Also, as seen on Fig. 3, the results of *Q4U3-AS* element for eigenvalues on the moderately coarse mesh (4x12) do not differ much from those obtained on 4-times denser mesh, concluding that the presented element is quite versatile and can be used in any modal analysis in practice with acceptable efforts in problem description.

5. Conclusion

A new finite element *Q4U3-AS* constructed on the assumed shear strain concept and derived from the starting cubic linked and problem dependent interpolations is presented. The element is tested on the dynamic benchmark problem of finding the eigenvalues for the circular plate of uniform thickness. The assessment on various element mesh densities is tested and the element is compared with other elements from the literature.

The new *Q4U3-AS* element has been validated in the presented dynamical analysis and will further be implemented as an element used in static or dynamic analysis of layered structures within the acknowledged research project.

Acknowledgement. *The results shown here have been obtained within the research project IP-06-2016-4775: "Assumed strain method in finite elements for layered plates and shells with application on layer delamination problem – ASDEL" financially supported by the Croatian Science Foundation from 2017.*

References

[1] T. Hughes i T. Tezduyar, »Finite Elements Based upon Mindlin Plate Theory with Particular Reference to the Four-Node Bilinear Isoparametric Element,« *Journal of Applied Mechanics,* pp. 587-596, 3 48 1981.

[2] R. H. MacNeal, »Derivation of Element Stiffness Matrices by Assumed Strain Distributions,« *Nuclear Engineering and Design,* pp. 3-12, 1 70 1982.

[3] K.-J. Bathe i E. N. Dvorkin, »A Formulation of General Shell Elements—the Use of Mixed Interpolation of Tensorial Components,« *International Journal for Numerical Methods in Engineering,* pp. 697-722, 3 22 1986. .

[4] D. Ribarić i G. Jelenić, »Higher-Order Linked Interpolation in Quadrilateral Thick Plate Finite Elements,« *Finite Elements in Analysis and Design,* pp. 67-80, 51 2012.

[5] D. Ribarić, "Problem-Dependent Cubic Linked Interpolation for Mindlin Plate Four-Node Quadrilateral Finite Elements," *Structural Engineering and Mechanics,* pp. 1071-1094, 6 59 2016.

[6] D. Ribarić, »Four-Node Plate Elements with Assumed Shear Strain That Satisfy the Patch Test,« u *8th International Congress of Croatian Society of Mechanics*, Opatija, 2015..

[7] D. Ribarić, "Higher-Order Linked Interpolation in Moderately Thick Plate and Facet Shell Finite Elements, PhD Thesis," Univrsity of Rijeka, Rijeka, 2012.

[8] O. Zienkiewicz and R. Taylor, The Finite Element Method, Fifth edition, Vulume 1: The Basis, Oxford: Butterworth-Heinemann, 2000.

[9] A. Tessler i T. Hughes, »A Three-Node Mindlin Plate Element with Improved Transverse Shear,« *Computer Methods in Applied Mechanics and Engineering,* svez. 50, p. 71–101, 1985.

[10] S. Lee, »Free Vibration Analysis of Plates by Using a Four-Node Finite Element Formulated with Assumed Natural Transverse Shear Strain,« *Journal of Sound and Vibration,* svez. 278, p. 657–684, 2004.

[11] T. Nguyen-Thoi, P. Phung-Van, H. Nguyen-Xuan i C. Thai-Hoang, »A Cell-Based Smoothed Discrete Shear Gap Method Using Triangular Elements for Static and Free Vibration Analyses of Reissner–Mindlin Plates.,« *International journal for numerical methods in Engineering,,* pp. 705-741, 7 91 2012.